EFDA–JET–PR(10)52

G. Telesca, R. Zagorski, S. Brezinsek, W. Fundamenski, C. Giroud,
G. Maddison, M. O' Mullane, J. Rapp, M. Stamp, G. Van Oost,
and JET EFDA contributors

Simulation with the COREDIV Code of Nitrogen Seeded H-mode Discharges at JET

Simulation with the COREDIV Code of Nitrogen Seeded H-mode Discharges at JET

G. Telesca[1], R. Zagorski[2], S. Brezinsek[3], W. Fundamenski[4], C. Giroud[4], G. Maddison[4], M. O' Mullane[4], J. Rapp[3], M. Stamp[4], G. Van Oost[1], and JET EFDA contributors*

JET-EFDA, Culham Science Centre, OX14 3DB, Abingdon, UK

[1]Department of Applied Physics, Ghent University, Plateaustr. 22, B-9000 Gent, Belgium
[2]Institute of Plasma Physics and Laser Microfusion, EURATOM/IPPLM Association, Warsaw, Poland
[3]IEF-4, FZ Jülich GmbH, Association EURATOM-FZJ, TEC, Jülich, Germany.
[4]EURATOM/CCFE Fusion Association, Culham, Abingdon, Oxon. OX14 3DB, UK.

** See annex of F. Romanelli et al, "Overview of JET Results", (23rd IAEA Fusion Energy Conference, Daejon, Republic of Korea (2010)).*

Preprint of Paper to be submitted for publication in
Plasma Physics and Controlled Fusion

ABSTRACT

The code COREDIV, self-consistent both with respect to the interaction plasma coreplasma edge and main plasma-impurities, is used to simulate nitrogen seeded JET discharges. The model is fully described and comparison of the numerical results is done with experimental data pertaining to two series of discharges different in input power, in confinement, in the level of the power radiated and in the puffing rate of the main gas and of nitrogen. Impurity sources, their transport and densities are considered as a function of the edge and core parameters and the consistency with the power they radiate is discussed. Special emphasis is given to the analysis of the fluxes of carbon and of the recycling fluxes of deuterium.

1. INTRODUCTION

One of the crucial and challenging issues of the fusion research in present days is the development of an ITER scenario which satisfies simultaneously the requirement of sufficiently high power amplification with that of sustainable power exhaust. Independently of techniques to mitigate the Edge Localized Modes, ELMs, and their impact on the plasma facing components, impurity seeding seems to be an unavoidable choice to limit to acceptable level the power load to the divertor plates of ITER and to reduce sputtering by edge radiation cooling. In view of possible realistic predictions for ITER-relevant scenarios with full carbon divertor and with impurity seeding, JET discharges with nitrogen injection have been numerically simulated in recent years using the self-consistent transport code COREDIV. The coupled core-edge code COREDIV [1,2] has been developed and benchmarked against JET discharges proving its capability of reproducing - with the diagnostic and modeling uncertainties - the main features of JET seeded plasmas [3]. Although global parameters as the electron temperature and density profiles in the plasma core, the total radiated power, Prad, and the ionic effective charge, Z_{eff}, of a variety of JET discharges were well reproduced with the COREDIV model – on this basis a preliminary extrapolation to ITER has been performed [4] - some aspects of the edge model of COREDIV were not fully developed and exhaustively tested, so far. These aspects, related mainly to the recycling fluxes of deuterium, to the mechanisms of carbon sputtering and to impurity transport, are considered in detail in the present study with the aim of providing a better understanding of the COREDIV edge model for JET discharges.

Since this work is also intended to provide the basis for modeling discharges of JET at low divertor load with the new ITER Like Wall (ILW), we have focused our interest on two nitrogen seeded scenarios, specially designed and developed at JET to fulfill the request of sustainable heat load : i) experiments with nitrogen seeding at high plasma current $I_p \sim 3$MA, high Greenwald fraction, power radiated fraction, f_{rad}, up to 0.75 and moderate confinements ($H_{98P(y,2)}$ in the range 0.65 – 0.75, Type III ELMs), see ref. [5] and ii) experiments at $I_p \sim 2.5$MA, medium-high Greenwald fraction, frad up to 0.63 and high confinement ($H_{98P(y,2)}$ in the range 0.8–1 0, Type I ELMs) [6,7].

The physical model implemented in the COREDIV code, described in the next section, and used in the simulations couples self-consistently radial 1D energy and particle transport equations of

plasma and impurities in the core region (up to the Last Magnetic Flux Surface, LMFS) and 2D multifluid transport in the scrape-off- layer, SOL. Since the energy and particle balance depends strongly on the coupling between the bulk and the SOL, modeling requires the transport to be addressed simultaneously in both regions. For reasons of simplicity, as explained in the next section, the plasma–wall interaction occurs only at the divertor plate which is the only place where the power is deposited and where intrinsic impurities are released from. The model accounts, also self-consistently, for the interaction between seeded impurities and intrinsic carbon.

In spite of the fact that COREDIV is intrinsically time dependent, the code was used so far to simulate the steady state phases of the discharges. Micro instabilities are accounted for in the prescribed level of the transport coefficients (see next section) while instabilities which may lead to Edge Localized Modes, ELMs, are herein not considered, as well as their impact on erosion, fluxes etc. In fact, the time dependent transport equations result in stationary profiles which have to be compared only to time-average values of the actual experimental plasma profiles.

In Section 2 the main structure of the transport model in COREDIV is described. In Section3 the numerical results are compared to JET experiments and Section.4 is devoted to the discussion of the results and to the conclusions.

2. THE SELF-CONSISTENT TRANSPORT MODEL IN COREDIV

Differently from other simulations with impurity seeding [8,9] in which the extrinsic impurities add to the intrinsic ones, the unique feature of our model consists in the selfconsistent interplay between the different impurities. In fact, each impurity affects the flux of the other impurities as well as the level of the power they radiate, due to changes each impurity causes in the local plasma density and temperature at the target, in the edge region and in the core. This non-linear interplay has been experimentally observed on TEXTOR and JET [10,11].

The problem of self-consistent modeling of the core and edge plasma has already been addressed in papers of Becker [9] and of Mandrekas/Stacey [8,12]. In our approach, for the plasma core we follow to a large extent the modeling assumptions in those papers, while a different model is used for the edge.

The core. The core part of our model, is based on a standard set of equations describing multifluid radial transport. The 1D radial transport equations for bulk ions, for each ionization state of impurity ions and for the electron and ion temperature are solved in the central part of the plasma. It is assumed that all ions have the same temperature. With respect to the energy sources, ohmic heating is calculated self-consistently with the plasma dynamics, whereas for auxiliary heating parabolic-like deposition profile is assumed.

The energy losses are determined by bremsstrahlung, synchrotron and line radiation. The electron and ion energy fluxes are defined by the local transport model proposed in Ref. [12] which reproduces a prescribed energy confinement law. In particular, the anomalous heat conductivity used in COREDIV for the simulations here presented is given by the expression

$$\chi_{e,i} = C_{e,i} \frac{a^2}{\tau_E} F(r) \qquad (1)$$

where τ_E is the energy confinement time given by the ELMy H-mode scaling law [13], a is the plasma radius, $C_i = C_e$ is a coefficient numerically determined to reproduce the prescribed value of the energy enhancement factor $H_{98P(y,2)}$ and F(r) is a profile function. F(r) is a parabolic function which might include a drop in the transport coefficients near the separatrix. In the simulations here presented we have adopted for F(r) a simple parabolic function.

The profile of the main plasma ion density is given by the solution of the radial diffusion equation with diffusion coefficient of the form

$$D_i = D_e = \alpha\chi_e \tag{2}$$

In simulations of experimental plasmas the value α of the ratio D_e/χ_e is chosen to reproduce the measured profiles. In our calculations we assume for a the value of 0.1. We point out, however, that the value of the ratio D_e/χ_e affects only weakly the results of our simulations. Indeed, our transport coefficients do not depend on local gradients and, thus, the resulting density profile is slightly modified by changes in the diffusion coefficient, since the particle flux is determined by the sources.

The profile of the source function takes into account the attenuation of the neutral density due to ionization processes:

$$S_i = S_{i0}\, exp(-\frac{a - r}{\lambda_{ion}}) \qquad r \le a \tag{3}$$

where λ_{ion} l is the penetration length of the neutrals, calculated self-consistently. Since the average electron density of the considered discharge is an input parameter in our model, the source intensity S_{i0} is determined by the internal iteration procedure in such a way that the average electron density obtained from neutrality condition equals that of the discharge considered.

In contrast with previous simulations, in the actual model of COREDIV the radial impurity transport is described by the simple and widely used analytical expression

$$\Gamma_z = D_\perp (\frac{dn_z}{dr} + S \cdot \frac{r}{a^2} \cdot n_z) \tag{4}$$

where Γ_z is the flux of impurities of charge Z, $D_\perp$ is the anomalous perpendicular main ion diffusivity, n_z is the impurity density and $S \sim \tau_E^2$. With this choice, the resulting inward impurity pinch is proportional to τ_E ($v_{pinch} \sim \tau_E\, r/a^2$) since in our transport model (please, see above) $D_\perp \sim 1/\tau_E$.

The edge. In COREDIV, the particle and energy fluxes coming from the bulk are calculated self-consistently with the SOL dynamics since the plasma transport in the core and in the SOL are solved simultaneously. This requires that the core and edge part of COREDIV are iterated alternatively until steady state is achieved. For each time iteration in the core, several time steps (10 – 20) are performed in the SOL to adjust the edge parameters. For that reason we have chosen a relatively simple SOL model, assuming slab geometry and neglecting drifts, however keeping the basic 2D

features of the edge plasma transport. In addition, we simplified the neutral model in order to avoid time consuming Monte Carlo iterations.

In COREDIV, for the SOL we use a 2D boundary layer model based on Braginskii-like equations [14,15,16] for the plasma and on rate equations for each ionization state of each impurity species. Since the radial transport is anomalous, the radial components of the Braginskii system of equations, and the related radial convective fluxes, are not considered, according to the ansatz that the radial transport is of diffusive nature. In fact, only the parallel component of the momentum equation is solved in COREDIV, consistently with the absence of drifts.

For every ion species the continuity, the parallel momentum and energy equations are solved and an analytical description of the neutrals allows to include deuterium recycling as well as the sputtering processes at the target plates. We assume that the divertor is in attached mode and the hydrogen recycling coefficient R is an external parameter, which varies in the present simulations in the range 0.975 - 0.983. The energy losses due to interactions with hydrogenic atoms (line radiation, ionization and charge exchange) are accounted for in the model. The mechanisms of carbon release consist of physical sputtering [17] as well as chemical sputtering, which is calculated according to the flux dependence expression of Roth [18]. Self-sputtering of carbon is included in the model while carbon sputtering by nitrogen ions is not considered in the model, so far. In Sect. 4 the quantitative implications for disregarding such a mechanism are estimated. Simple slab geometry (along field lines and radial direction) with classical parallel transport and anomalous radial transport (given as an input, normally $0.5 m^2/s$) is used and the impurity fluxes and radiation losses caused by intrinsic and seeded impurity ions are calculated fully self-consistently. The standard sheath boundary conditions are imposed at the plates, whereas at the wall the boundary conditions are given by decay lengths. The parallel velocities and the gradients of densities and temperatures are assumed to be zero at the midplane (stagnation point).

3. EXPERIMENTS AND SIMULATIONS

In this section, experimental data are compared with COREDIV simulations. Comparison experiment-simulation for the particle fluxes is a rather critical issue because, on top of the usual uncertainties related to the spectroscopic determination of the photon fluxes (absolute calibration, assumed symmetries), the experimental evaluation of particle fluxes needs the ionization per photon (S/XB) to be assigned. This number, which depends strongly on the local temperature and density, can be determined only with some approximation and, in principle, should be different for each pulse [19]. Following [20] we have assigned both for the D_α and for CII line (λ = 515nm), S/XB = 30 for the outer divertor and S/XB = 15 for the inner divertor for the pulses at high confinement (Sect ion 3.2). For the pulses at high density (Sect.3.1) we keep S/XB = 30 for the outer divertor and S/XB = 15 for the inner divertor for the CII line, but we have assigned S/XB = 15 for the outer divertor and S/XB = 7.5 for the inner divertor for the D_α line. We did this choice in consideration of the very low edge temperatures for the discharges at high density (~ 5eV, please see next section),

3.1. TYPE III DISCHARGES WITH N2 SEEDING AT HIGH ELECTRON DENSITY.

This series of Type III ELMy discharges [5,21] consists of a power scan from 16MW to 24MW at high plasma current (I_p = 3MA), high density plasmas (central line-average electron density, n_e, in the range 0.92 – 1.07 x 10^{20} m^{-3}) with highly radiative fraction (f_{rad} up to 0.75, i.e. up to 17MW) and $H_{98P(y,2)}$ in the range 0.65 - 0.75. The input power is mainly provided by NBI with 2-3 MW of ICRF heating. For this series, the recycling coefficient in COREDIV has been set to R = 0.975.

Probe data are not available for this series of pulses, however the COREDIV simulations compute for these discharges the electron temperature at the plate, T_e(pl), on the order of 4-5 eV, with the exception of the discharge at the highest input power (P_{aux} = 24MW), for which, due also to the slightly lower electron density, T_e (pl) is calculated to be about 11eV. In figure 1 the experimental and simulated D recycling fluxes (top) and C fluxes (bottom) are shown as function of the auxiliary power level. With respect to the absolute value of the experimental D fluxes (i.e. with respect to the value we have assigned to the S/XB to estimate the experimental D fluxes), one can observe that the boundary condition $Q^{div} = Q^{heat}(1\text{-}f_{rad}) = 8 \times \Gamma_e T_e(plate)$ would imply that T_e at the plates is about 5–6eV for $\Gamma_e = 6–8 \times 10^{23} s^{-1}$ when the typical value (experimental) of the power load Q^{div} = 5MW is used. Particle flux level much higher than that would lead to lower temperature at the plates, incompatible with the attached plasmas we are referring to. On the other hand, measurements performed for similar nitrogen seeded JET pulses, and reported in ref. [22], indicate an electron temperature at the plates of about 5eV. With respect to the carbon fluxes, it is worth noting that for such low edge temperature plasmas, chemical sputtering is the dominant carbon release mechanisms. Physical sputtering can contribute to the C fluxes only for the pulse at T_e(pl) = 11eV, the pulse at P_{aux} = 24MW, as might be noticed comparing the simulated D and C fluxes in Fig.1. The experimental and simulated P_{rad} and Z_{eff} compare very well (Fig.2) as do the experimental (Charge Exchange Recombination Spectroscopy, CXRS) and simulated concentrations of fully stripped nitrogen in the plasma core. According to (4), for these low confinement, highly diffusivity plasmas the impurity peaking factor ($= -v_{pinch}/D_\perp \sim \tau_E^2$) is marginal ($< 0.3$ m^{-1}) and practically does not affect carbon and nitrogen transport, in agreement with previous studies of impurity transport in presence of ICRF heating

3.2. TYPE I DISCHARGES WITH N2 SEEDING.

These discharges [6, 7, 24], expressly developed in preparation of the ILW with full W divertor, consist of a systematic scan of D puffing rate at a given level of N seeding and of a systematic scan of N seeding at a given level of D puffing rate. For all the discharges, the total input power is about 16MW, about 2 of them provided by ICRF heating. Keeping the N puffing at $\Gamma_N^{puff} = 4.8 \times 10^{22}$el/s, the D puffing changes in the range $1.2–2.8 \times 10^{22}$el/s and keeping $\Gamma_D^{puff} = 2.8 \times 10^{22}$el/s, Γ_N^{puff} changes in the range $0–4.8 \times 10^{22}$el/s.

At $\Gamma_N^{puff} = 4.8 \times 10^{22}$el/s, increasing the D puffing from 1.2 to 2.8×10^{22}el/s , the central line-average electron density ne increases from 5.7 to $7.6 \times 10^{19} m^{-3}$ and the confinement enhancement factor $H_{98P(y,2)}$ decreases from 0.95 to 0.82. At $\Gamma_D^{puff} = 2.8 \times 10^{22}$el/s, decreasing the N puffing rate

from $\Gamma_N^{puff} = 4.8 \times 10^{22}$el/s to zero, ne increases from 7.6 to 10×10^{19} m^{-3} and $H_{98P(y,2)}$ increases from 0.82 to 1.0.

Since the level of D puffing affects the electron density as well as the recycling coefficient, R, see Ref. [6,7], we have used different R when computing pulses with different experimental D puffing rates: increasing the experimental D puffing rate from $\Gamma_D^{puff} = 1.2 \times 10^{22}$el/s to $\Gamma_D^{puff} = 2.8 \times 10^{22}$el/s, we have increased in COREDIV therecycling coefficient from 0.975 to 0.983 (please, recall that in COREDIV the recycling is an external input parameter). As a preliminary test, we have estimated the effects of a change in R on some discharge parameters by doing numerical simulations for one of the pulses of this series in which only R was changed, keeping unchanged all the others input parameters. As can be seen in Fig. 3 the effect of changing R in COREDIV is minimal both on P_{rad} and in Z_{eff}, although a significant effect is seen on the edge temperature and on the D recycling flux leaving, however, their product nearly constant.

In figure 4, the experimental and simulated D and C fluxes are shown for the D puffing scan. Comparing experiment with simulation, either the experimental D flux at the lower D puff is too low or those at higher puffing are too high. This is consistent with the fact that for the lower D puffing (low density) the calculated T_e(pl) is on the order of 30eV while for the remaining two points (higher density) the calculated T_e(pl) is on the order of 10eV. Therefore the S/XB for the pulse at low D puffing should be higher than that for the pulses at high puffing, rendering higher the "experimental" D flux. Very similar considerations can be made for the comparison experiment-simulation for the carbon fluxes. Considering the N seeding scan, Fig, 5, since the edge temperatures are rather similar to each other, the discrepancy simulation-experiment at the point $\Gamma_N^{puff} = 0$ for the carbon flux is likely related to the presence of a small amount nitrogen in the experimental pulse, assumed in the simulation to be without nitrogen (see below). The presence of N in a real discharge, indeed, might reduce the level of carbon flux, see refs. [10, 22].

The experimental and simulated P_{rad} and Z_{eff} are shown in Fig.6 as function of the D puffing rate and in Fig.7 as a function of N seeding. With respect to the D puffing scan, while P_{rad} remains nearly constant with increasing D puffing, Z_{eff} decreases as a consequence of the increase in the electron density and of the decrease in confinement (in impurity inward pinch). With respect to the simulated value of P_{rad} for the N seeding scan at $\Gamma_N^{puff} = 0$ (large discrepancy with the experimental value), one can consider that the presence of a small amount of N (few per mille) would lead in the numerical result to a significant increase of P_{rad} (hundreds of kilowatts), due to the high value of the electron density and to the rather good radiation properties of nitrogen in the considered range of temperatures, while would hardly affect Z_{eff}. Indeed, nitrogen legacy, which is generally observed to occur on JET during these experiments [6, 22], has quite recently been confirmed by CXRS [25]. The numerical decomposition of Z_{eff} in carbon and nitrogen concentration (Fig.7, bottom), which shows changes in carbon concentration in the presence of nitrogen, reflects the interplay of different impurities, accounted for in COREDIV. Such an interplay has experimentally been observed [6,10]. In Fig.8a it is shown the COREDIV decomposition of the total radiation path inside the separatrix

for the pulse at $\Gamma_N^{puff} = 0$ and in Fig. 8b for that at the highest N puffing rate. For the pulse at $\Gamma_N^{puff} = 4.8 \times 10^{22}$el/s (Fig. 8b) the carbon edge radiation decreases by about a factor of two as compared to the unseeded case, in parallel with the decrease in carbon concentration seen in Fig. 7, bottom. The remaining edge radiation inside the separatrix is provided by nitrogen, while bremsstrahlung is responsible for about one megawatt (for both pulses) of power radiated in the more central plasma.

For these Type I ELMy pulses, the simulated impurity peaking ($-v_{pinch}/D_\perp$) is in the range 0.4 – 0.6m^{-1}. Even though this value is modest, it does affect impurity transport leading to Z_{eff} levels higher, on the average, than those for the Type III pulses.

4. DISCUSSION AND CONCLUSION

In spite of the difficulties related to the absolute determination of the experimental D and C fluxes, the comparison experiment-simulation appears to be rather satisfactorily. Indeed, the trends experiment-simulation are similar while the major differences might reasonably be related to the simple method used to determine the experimental fluxes. In fact, the differences experiment-simulation are within 20-30% when comparing series of discharges with similar edge temperatures (as the ones in 3.1 and the N puffing scan in 3.2), while can increase up to more that a factor of two when comparing experiment-simulation for pulses with a large spread in the edge temperatures. One exception is the C flux for the N scan in 3.2 at $\Gamma_N^{puff} = 0$ (Fig.5) for which we have assumed zero N flux in COREDIV while recent spectroscopic data [25] would indicate the presence of some amount of nitrogen in this discharge. The presence of N is, in general, accompanied with a decrease of the carbon flux, which would explain the lower C flux in the experimental data, as compared to simulation. These results indicate that the COREDIV model for the main gas recycling and for carbon sputtering is substantially correct and that COREDIV reflects with sufficient accuracy the underlying physical mechanisms. This is especially relevant for carbon, considering that for the Type III ELMy series the chemical sputtering is the main carbon release mechanism, while for the Type I ELMy series physical sputtering is the dominant one.

In the present model of COREDIV, carbon sputtering caused by impinging nitrogen on graphite is not taken into account. However, we can estimate that the contribution of this carbon release mechanism is relatively modest for the considered experiments. Indeed, considering that carbon self-sputtering, which is included in COREDIV, accounts in the simulations of these pulses for a few percent of the total carbon flux and that the concentrations of C and N are similar (in the range 1–2.5%, see Figs.2 and 7), and considering also the similarities of C and N, the resulting numerical underestimation in the total carbon release can reasonably be assumed to be of the same order, of a few percent.

The simplified geometry of the SOL in COREDIV does not allow to take into account carbon released from the wall, which has been shown in ref. [26] to enter the plasma core more easily than that released at the target. The related error is, however, minimized by two facts: first, in the experiments, the carbon release from the wall is a small fraction of the total carbon flux [26] and,

second, in COREDIV the ions produced at the target can be transported by thermal forces into the far SOL where they fuel the core with increased efficiency.

As a last point, we note that the quantity P_{rad} / [(Z_{eff} -1) n_e^2 2] is, on the average, higher for the Type III ELMy discharges than for the Type I ELMy ones, both in experiments and in simulations: it is about 1.8×10^{-39} [MW m6] for Type III and about 1.2×10^{-39} [MW m^6] for Type I. This quantity can be expressed as a function of the cooling rates (it increases with decreasing the edge temperature, for C and N) and of the impurity transport (it increases with decreasing the impurity dwell time) [27]. In the Type III series the edge temperatures are low as it is the inward pinch, while in the Type I series the temperature are higher, as it is the inward pinch. This contributes to confirm the global internal selfconsistency of the numerical reconstruction of these discharges.

In conclusion, in spite of the limitations caused by the uncertainties in the measurements as well as in the simulations and in spite of the limitations caused by the oversimplified SOL model, the results presented in this paper show the capability of the COREDIV model of reproducing the main features of nitrogen seeded H-mode JET discharges with moderate power load on the carbon divertor. In particular, the acceptable agreement experiment-simulation found for the level of the carbon flux and for that of its density in the core, and/or Z_{eff}, (see, for instances, Figs. 1 and 2) implies that the impurity transport model we have adopted is substantially correct.

This gives us some confidence in the viability of modeling with COREDIV the impurity seeded discharges of JET with the new ILW.

ACKNOWLEDGEMENTS.

This work was supported by the EURATOM and carried out within the framework of the European Fusion Development Agreement. The views and opinions expressed herein do not necessarily reflect those of the European Commission.

REFERENCES

[1]. R. Zagorski and R. Stankiewicz, Journal of Nuclear Material. **313-316** (2003) 899

[2]. R. Stankiewicz and R. Zagorski, Journal of Nuclear Material **337-339** (2005) 191

[3]. R. Zagorski et al., Contribution to Plasma Physics. **48** (2008) Issue 1-3, 179

[4]. G. Telesca et al., Nuclear Fusion **47** (2007) 1625

[5]. J. Rapp et al., Journal of Nuclear Materials. **390-391** (2009) 238

[6]. G. Maddison et al., "Impurity seeding experiments on JET in preparation for the ITER like wall", 36th EPS Conference on Plasma Physics., Sofia, June 29-July 3- 2009, ECA Vol. **33** E, P-2.160 (2009)

[7]. G. Maddison et al., " Moderation of target loads using fuelling and impurity seeding on JET in preparation for the ITER-like wall " Paper O-23, 19th PSI Conference, San Diego, Ca, USA, 24-28 May 2010, to be published in Journal of Nuclear Materials

[8]. J. Mandrekas et al., Nuclear Fusion **37** (1997) 1015.

[9]. G. Becker, Nuclear Fusion **38** (1998) 293.

[10]. G. Telesca et al., Nuclear Fusion **36** (1996) 347.
[11]. J. Rapp et al., Journal of Nuclear Materials. **337-339** (2005) 826.
[12]. J. Mandrekas and W.M. Stacey, Nuclear Fusion **35** (1995) 843.
[13]. V. Mukhovatov et al., Plasma Physics and Controlled Fusion **45** (2003) A235.
[14]. H. Gerhauser et al., Nuclear Fusion **42** (2002) 805.
[15]. S.I. Braginskii, Review of Plasma Physics. 1 (1965) 205.
[16]. R. Zagórski et al., Contribution to Plasma Physics., **38**, No.1-2 (1998) 6.
[17]. Y. Yamamura et al., Report of the IPP Nagoya, IPPJ-AM-26
[18]. J. Roth et al., Nuclear Fusion **44** (2004) L21.
[19]. http://www.adas.ac.uk
[20]. S. Brezinsek et al., Plasma Physics and Controlled Fusion **47** (2005) 615-634
[21]. G. Telesca et al., "Progress in COREDIV modeling of impurity seeded JET discharges" 36th EPS Conference on Plasma Physics , Sofia, June 29-July 3- 2009, ECA Vol. 33E, P-2.163 (2009).
[22]. S, Brezinsek et al., "Impact of nitrogen seeding on carbon erosion in the JET divertor" , accepted for publication in Journal of Nuclear Materials 14
[23]. L. Carraro et al., "Impurity profile control in JET plasmas with radio-frequency power injection", 34th EPS Conference on Plasma Physics, Warsaw, ECA Vol 31F O-4.028 (2007)
[24]. G. Telesca et al., "Modeling of plasma fuelling and nitrogen seeding of JET discharges with the COREDIV code", 37th EPS Conference on Plasma Physics, Dublin, Ireland,21-25 June 2010, Paper P2.163.
[25]. C. Giroud et al., "Integration of a radiative divertor for heat load control into JET operational scenarios", 23rd IAEA Fusion Energy Conference, Daejon, Republic of Korea, 10-14 Oct. 2010, Paper EXC/P3-02.
[26]. J.D. Strachan et al., Nuclear Fusion **43** (2003) 922
[27]. G .Telesca et al., Journal of Nuclear Materials. **241-243** (1997) 853

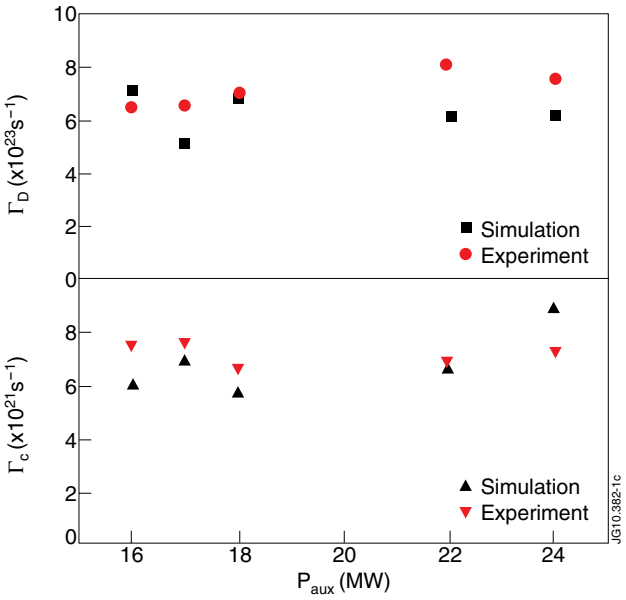

Figure 1: Experimental and COREDIV computed D recycling fluxes (top) and C fluxes (bottom) as a function of the auxiliary power.

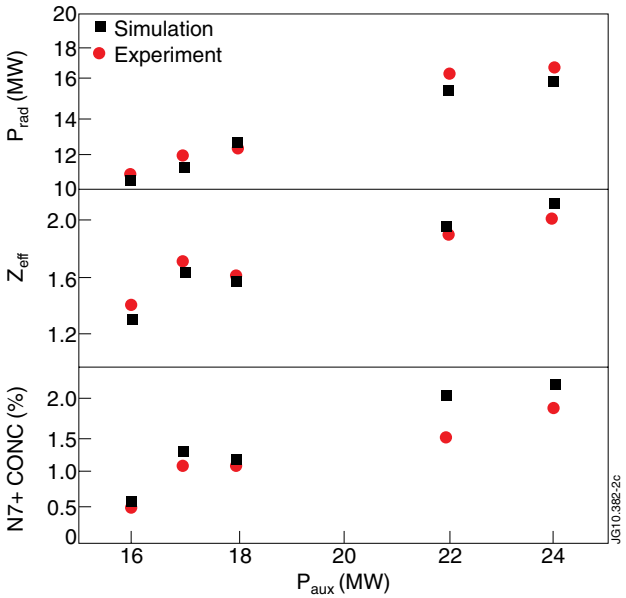

Figure 2: From top to bottom: experimental and COREDIV computed radiated power, Z_{eff} and nitrogen concentration in the plasma center.e.

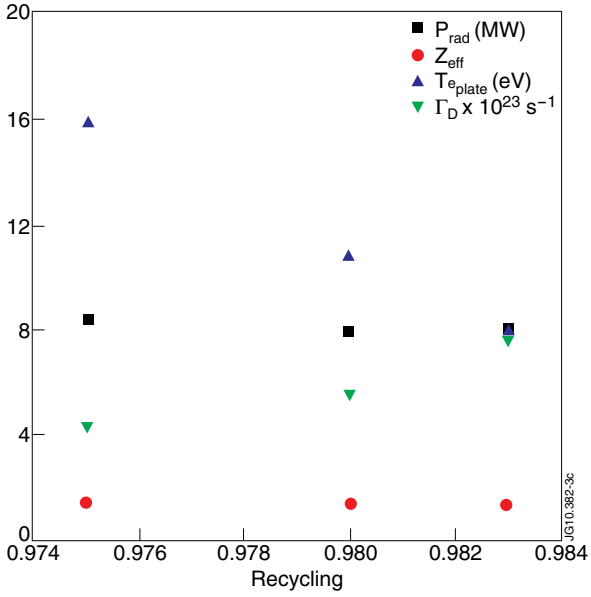

Figure 3: Simulated P_{rad}, Z_{eff}, $T_e(pl)$ and D recycling fluxes as a function of a change in the recycling coefficient.

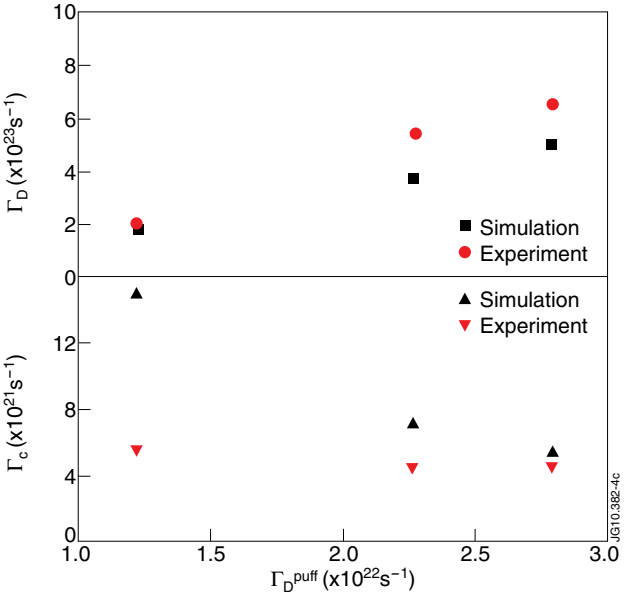

Figure 4: Experimental and computed D recycling fluxes (top) and C fluxes as a function of D puffing rate. Please, see text for comments.

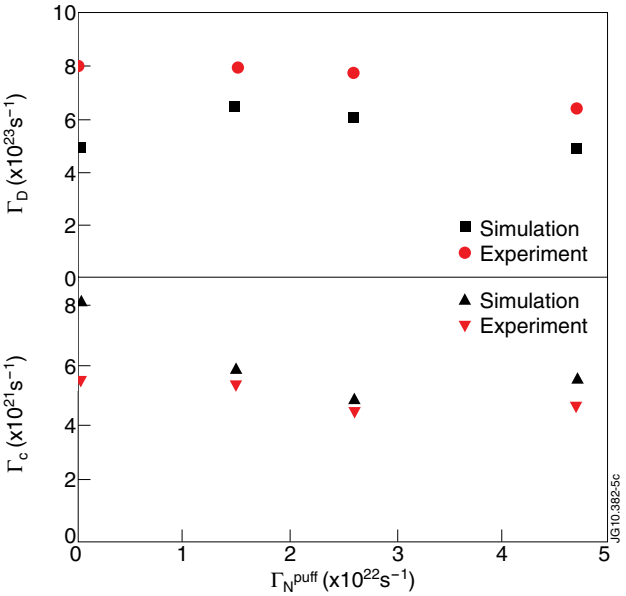

Figure 5: Experimental and simulated D recycling fluxes (top) and C fluxes (bottom) as a function of nitrogen puffing rate.

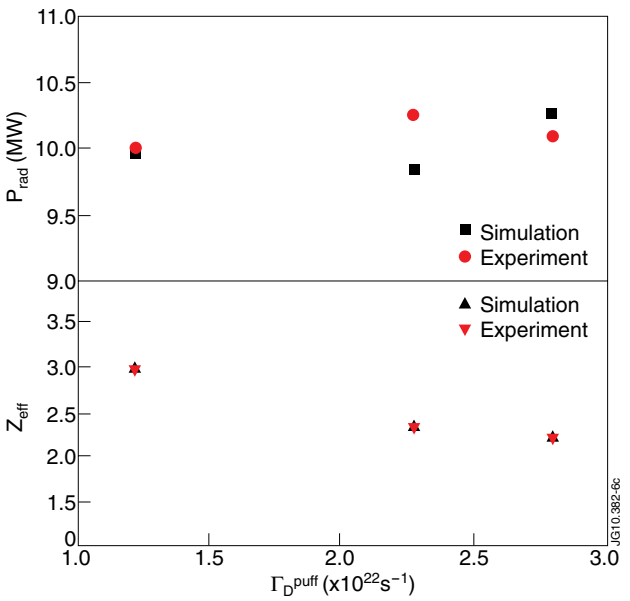

Figure 6: Experimental and simulated P_{rad} (top) and Zeff (bottom) as a function of D puffing rate for the Type I ELMy discharges.

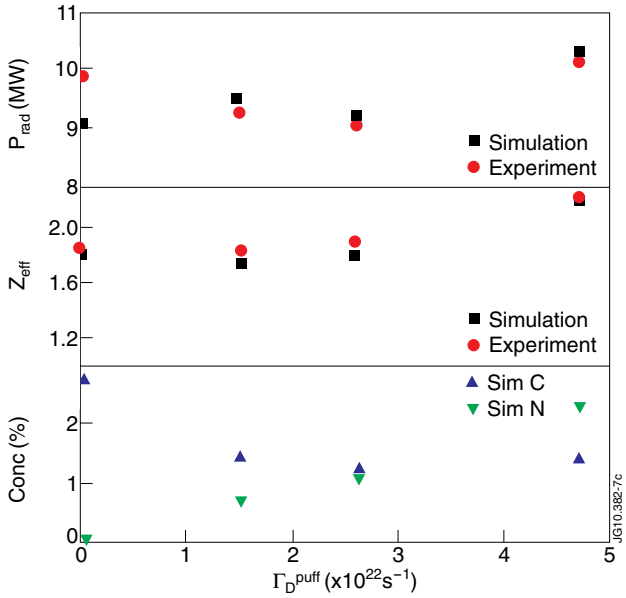

Figure 7: From top to bottom: experimental and simulated P_{rad}, Z_{eff} and numerical decomposition of Z_{eff} in C and N concentrations as a function of N puffing rate for the Type I ELMy discharges

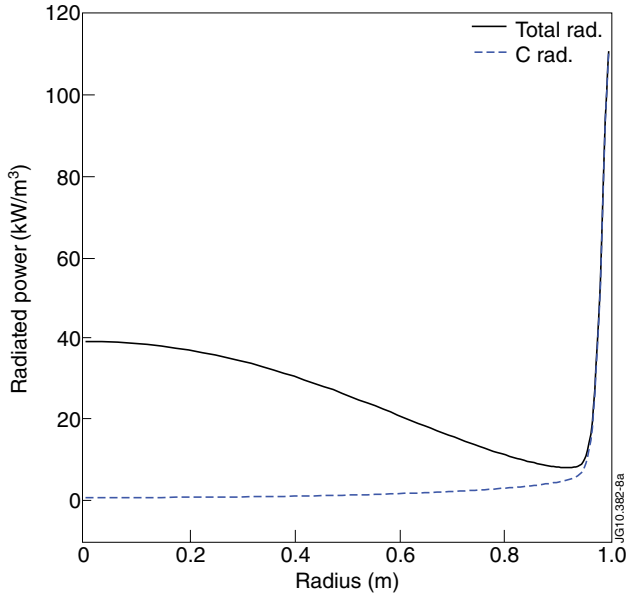

Figure 8a: COREDIV simulated profiles of the radiated power density inside the separatrix for the unseeded pulse of the Type I ELMy series.

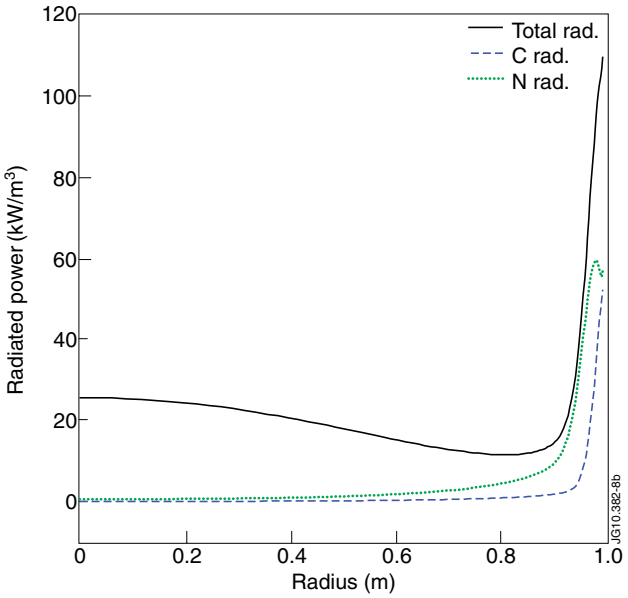

Figure 8b: COREDIV simulated profiles of the radiated power density inside the separatrix for the pulse at the highest nitrogen seeding level of the Type I ELMy series.